Theor Chem Acc (1997) 97:283–288

Theoretical
Chemistry Accounts


# Electronic structure of axially ligated rhodium carboxylates: $\pi$ back-bonding revisited

**Andrew L. Sargent**[1], **Mark E. Rollog**[1,*], **Cassandra T. Eagle**[2]

[1] Department of Chemistry, East Carolina University, Greenville, NC 27858, USA
[2] Department of Chemistry, Appalachian State University, Boone, NC 28608, USA

Received: 13 December 1996 / Accepted: 18 March 1997

**Abstract.** Fenske-Hall molecular orbital calculations have been applied to a new, structurally isolable analog of the intermediate involved in catalytic rhodium carboxylate carbenoid transformations. Results from the structural characterization of axially ligated rhodium acetate phenylisonitrile complexes have been utilized in approximate molecular orbital calculations. The results from the calculations suggest that a significant degree of $\pi$ back-bonding exists between the metal and isonitrile fragments which, by analogy, implies that $\pi$ back-bonding should also exist in the rhodium carbenoid intermediate. Sensitivity of the Fenske-Hall method to the magnitude of $\pi$ back-donation in these complexes was gauged through calculations involving different phenylisonitrile groups in which the $\pi$ back-bonding ability was modulated through derivativization. The reliability of the Fenske-Hall method was evaluated through a comparison to a high-level calculation.

**Key words:** Rhodium carboxylates – $\pi$ Back-bonding – Carbenoid transformations – Axial ligation – Fenske-Hall

## 1 Introduction

Rhodium carboxylates and carboxamides are important catalysts for a variety of carbenoid transformations [1], including cyclopropanations [2], N—H [3] and C—H [4] insertion reactions and dipolar cycloadditions [5]. These rhodium carboxylates and carboxamides have been modified extensively to enhance and direct chemical reactivity, diastereoselectivity and enantioselectivity. A question of vital importance to the rational design of selective catalysts is the structural and electronic makeup of the rhodium carbenoid intermediate. Despite the intense interest in these catalysts, little is known about the rhodium carbenoid species itself due, largely, to its highly transient nature.

The debate regarding the presence or absence of $\pi$ back-bonding in rhodium carboxylate complexes dates back to the original debates regarding the Rh—Rh bond order of such complexes [6]. While the Rh—Rh bond order is now firmly established as one, the debate regarding $\pi$ back-bonding, particularly in rhodium carbenoid complexes, is as yet unresolved [7]. Crystal field theory predicts that $\pi$ back-bonding would occur through donation of electron density from one of the degenerate metal $\pi^*$ orbitals into the vacant and unhybridized $p$ orbital of the carbene. Consequently, the expected conformation of the carbene would be one in which it eclipses the carboxylate ligands surrounding the metal core.

In an elegant series of linear free energy relationship experiments, Pirrung and Morehead demonstrated the importance of the polarizability and resonance contributions of the carboxylate (and carboxamide) ligands to the reaction selectivity in carbenoid transformations [7]. Their results suggest that $\pi$ back-bonding is an important facet of these transformations. Results of spectroscopic studies, published in the same report, indicate that $\pi$ back-bonding is important in $Rh_2(O_2CR)_4 \cdot CO$ complexes and, by analogy, in rhodium carbenes.

Doyle and co-workers, on the other hand, have proposed that a carbenoid intermediate exists which is devoid of $\pi$ back-bonding, and thereby contains a formal Rh—C single bond [8]. The electrophilic carbon is therefore more akin to a carbocation than it is to an alkylidene complex. Doyle based this proposition on modeling studies of chiral rhodium carboxamide complexes where the geometries were optimized with molecular mechanics calculations and the axial carbene ligand was subsequently rotated as a rigid rotor. In addition, each rotamer was examined with extended Hückel calculations. Results from both levels of theory suggested that the rotational barrier was less than 1 kcal/mol and supported their contention that the Rh—C bond lacks double bond character.

In another computational study, Bursten and Cotton performed X$\alpha$-SW calculations on the bisphosphine ad-

*American Chemical Society – Petroleum Research Fund Scholar
*Correspondence to*: A.L. Sargent

duct of rhodium formate [9]. The $Rh_2(O_2CH)_4 \cdot (PH_3)_2$ geometry was obtained from the X-ray crystal structure of the corresponding rhodium acetate adduct. The results of their calculations failed to show the presence of any significant $\pi$ back-donation from the metal to the phosphines. Bursten and Cotton do acknowledge, however, that the applicability of these results to other $\pi$-acid complexes is limited.

To shed further light on the structural composition of rhodium carbenoid complexes, a new model which involves rhodium acetate coordinated to a pair of isonitrile ligands was employed. The isonitrile group possesses $\sigma$ bonding and $\pi$ back-bonding capabilities similar to those of a carbene. Unlike the metal carbene adduct, however, the rhodium acetate isonitrile complexes are isolable, thus making structural studies possible.

Herein we report a theoretical analysis of the electronic structure and bonding of two rhodium acetate isonitrile complexes, $Rh_2(O_2CCH_3)_4 \cdot (CNC_6H_4CF_3)_2$, **1**, and $Rh_2(O_2CCH_3)_4 \cdot (CNC_6H_4N(CH_3)_2)_2$, **2**, using the Fenske-Hall molecular orbital method.

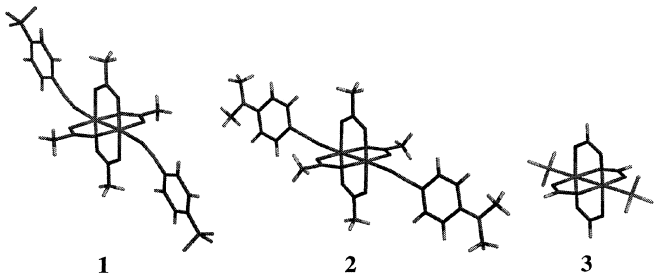

**1** **2** **3**

In addition, we re-investigate the electronic structure and bonding of $Rh_2(O_2CH)_4 \cdot (PH_3)_2$, **3**, with the Fenske-Hall method to provide a means through which the results of the present study can be compared to those from previous studies.

## 2 Methods

Unparameterized Fenske-Hall molecular orbital (MO) calculations [10] were utilized to examine the electronic structure and bonding in a variety of axially ligated rhodium carboxylates. The geometric parameters for **1** and **2** were taken directly from the X-ray crystallographic data (which will be reported in a subsequent paper), while those for **3** were taken from a previous study [9]. The basis functions for all non-hydrogen atoms were generated from the numerical X$\alpha$ atomic orbital program of Herman and Skillman [11], which was used in conjunction with the X$\alpha$-to-Slater basis program of Bursten and Fenske [12]. Non-transition metal atoms assumed ground-state atomic configurations, while the $s^0d^8$ cationic configuration was used for the Rh atom. The exponents for the valence $s$ and $p$ orbitals of Rh were determined by minimizing the energy difference between the valence eigenvalues obtained from the molecular calculations and experimental ionization potentials. The numerical X$\alpha$ atomic orbitals were fit to double-$\zeta$ analytical Slater type functions for the valence $d$ orbitals of Rh and for the valence $p$ orbitals of the other atoms except hydrogen, the exponent of which was 1.20. All other orbitals, including the $d$ polarization functions on P, were fit to single-$\zeta$ functions. A Mulliken population analysis [13] was used in the calculations to determine gross and overlap populations. The Mulliken gross populations, which were calculated following the transformation of the results in the atomic orbital basis to an MO basis of the chemically meaningful fragments, were employed to assist our analysis of the direction of electron density flow between interacting fragments.

An ab initio DFT/B3LYP SCF calculation of **3** utilized a modest-sized all-electron rhodium basis with a (4322/4221/331) contraction [14], a 6-31G* phosphorus basis, and a 6-31G basis for the remaining atoms and was performed through the GAUSSIAN 94 program package [15]. Contour and deformation density plots were created with an in-house version of MOPLOT [16].

## 3 Results and discussion

When the primary focus of a computational study is the interaction between two or more distinct chemical moieties, it is often useful to represent the results of the calculations in a basis of the MOs of these distinct moieties rather than in the usual basis of atomic orbitals for the conglomerate species. The distinct chemical moieties in this study are the rhodium acetate and the axial ligands. In Fig. 1, which shows the results of the Fenske-Hall calculation on **1**, the relevant valence MOs of rhodium acetate are shown on the left side of the diagram while those for the two isonitrile groups are shown on the right side. For the isonitrile species, each MO appears as a nearly degenerate pair, corresponding to the symmetric and antisymmetric combination of each MO on the two spatially separated isonitrile groups. The corresponding fragment molecular orbitals (FMOs) are labeled according to their $C_i$ symmetry designation. For the rhodium acetate fragment, the valence MOs closely resemble those of rhodium formate described previously in detail [6c], and exhibit the familiar $\sigma^2\pi^4\delta^2\pi^{*4}\delta^{*2}$ configuration. For consistency with the earlier reports [6c, 9], these FMOs are labeled according to their $D_{4h}$ symmetry designation. The MOs of **1** are labeled sequentially and without the $C_i$ symmetry designation to avoid confusion with the isonitrile FMOs, which have the same symmetry.

Prior to the interaction of the molecular fragments, all rhodium acetate and isonitrile FMOs below and including the $2b_{1u}$ and $1a_g$ orbitals, respectively, have an occupancy of 2.00, while the occupancy of the other FMOs is 0.00. Figure 1 shows that following the interaction of the fragments, the isonitrile $2a_g$ and $4a_g$ FMOs gain 0.10 and 0.11 electrons, respectively, from the rhodium $5e_g$ FMOs. These results suggest that a significant degree of $\pi$ back-donation exists. The amount of density back-donated from the rhodium $6e_u$ FMOs to the isonitrile $2a_u$ and $4a_u$ FMOs is much smaller (0.05 and 0.04 electrons, respectively) due to the larger energetic separation between these interacting fragments (vide infra). Figure 2a and b shows contour plots of the

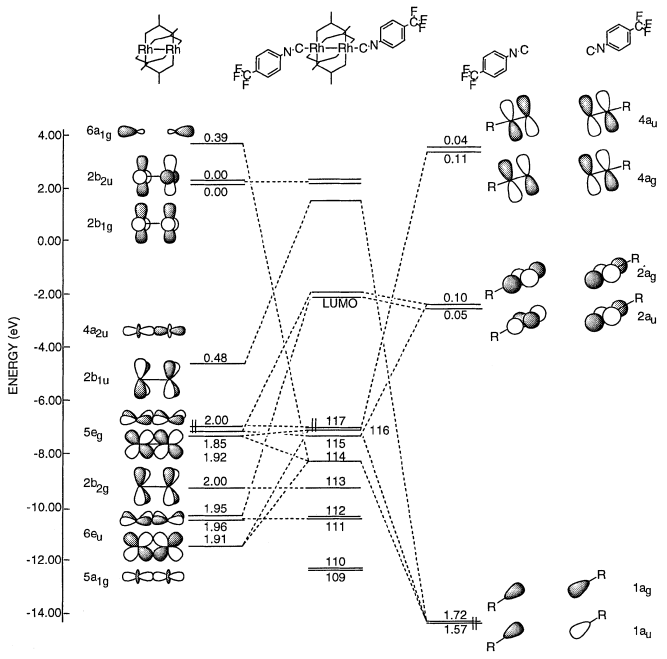


**Fig. 1.** Molecular orbital (MO) diagram for **1** showing the interaction between the $Rh_2(O_2CCH_3)_4$ and $(CNC_6H_4CF_3)_2$ fragments. Mulliken gross populations are listed adjacent to the corresponding fragment molecular orbital

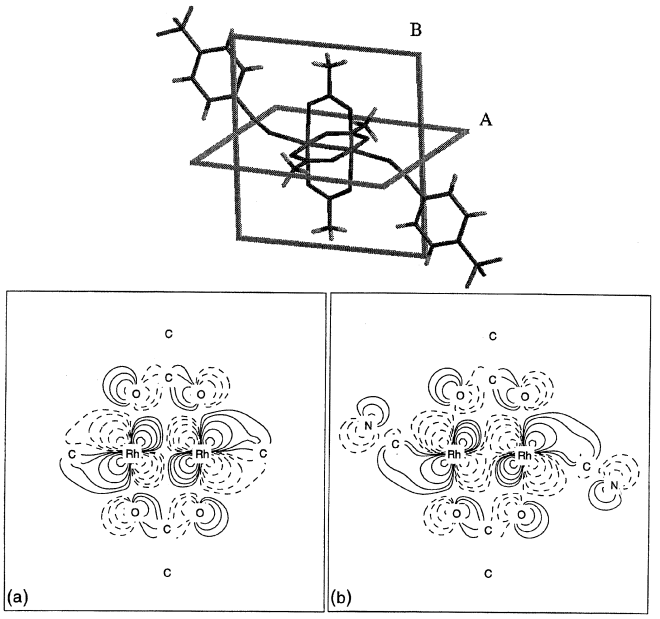


**Fig. 2a, b.** Contour plots for selected MOs of **1**. The *A* and *B* planes are shown in the top diagram of the figure. **a** MO 115 in plane *A*. **b** MO 116 in plane *B*. Contours are geometric, differing by a factor of 2, with the lowest contour of $\pm 0.01563(\text{e/a.u.}^3)^{1/2}$

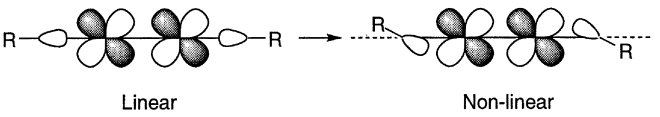


**Fig. 3.** Illustration of the metal-ligand $\pi$-$\sigma$ overlap as a function of axial ligand linearity with the metal-metal bond axis

MOs of **1** which encompass the bulk of the $\pi$ back-bonding interaction. In MO 115, shown in Figure 2a, the polarization of the Rh—Rh $\pi^*$ orbital away from the center of the molecule is evident. This polarization accentuates the overlap with the $2a_g$ FMO of the axial ligands. Notice that while the isonitrile carbon atoms reside slightly above and below the plane designated A in Fig. 2, their contributions can still be seen. The corresponding nitrogen atoms, however, are too far removed from the plane to be observed.

The $2a_g$ and $2a_u$ isonitrile $\pi^*$ FMOs are energetically stabilized by the $\pi$ system of the phenyl groups, which means that a better energetic match exists between these FMOs and the occupied metal FMOs than between the $4a_g$ and $4a_u$ isonitrile $\pi^*$ FMOs and the metal FMOs. This better match in energy translates into a stronger interaction between the fragments, according to the equation which quantifies the extent to which atomic or molecular fragments interact: the second-order perturbation correction to the molecular energy, Eq. (1). The numerator of this expression, which is the square of the Fock matrix

$$E_i^{(2)} = \sum_{j \neq i} \frac{|H_{ij}|^2}{E_i - E_j} \tag{1}$$

element, depends primarily on orbital overlap, while the denominator represents the difference in energy between the interacting FMOs. Assuming that a similar degree of overlap exists between the two sets of isonitrile $\pi^*$ FMOs and the metal FMOs, the smaller energy splitting between the $2a_g/2a_u$ set and the metal FMOs should enhance the interaction between these fragments and result in greater $\pi$ back-donation. The Mulliken gross populations listed in Fig. 1, however, indicate that the $\pi$ back-bonding to the $4a_u/4a_g$ FMOs is at least as strong as that for the $2a_g/2a_u$ FMOs despite the additional 6.0 eV separation in energy. An explanation for this apparent discrepancy follows.

Figure 1 shows that, in addition to the Rh—Rh $\pi^*$ interaction with the $4a_g$ isonitrile FMO, MO 116 of **1** contains significant contributions from FMOs $5a_{1g}$ and $1a_g$ of the rhodium and isonitrile fragments, respectively. These FMOs participate in the interaction largely as a consequence of the non-linear orientation of the axial groups with respect to the metal–metal internuclear axis. While the deviation from linearity decreases the Rh—isonitrile $\pi-\pi$ overlap, it *increases* the Rh—isonitrile $\pi-\sigma$ overlap, as illustrated in Fig. 3. The contributions from both the $5a_{1g}$ and $1a_g$ FMOs are easily seen in the metal–metal and metal–ligand regions of the contour plot of MO 116, shown in Fig. 2b. The participation of these FMOs results in the symmetry allowed redistribution of electron density from $\sigma$ FMOs such as the rhodium $5a_{1g}$ into the isonitrile $4a_g$ FMO.

Figure 4a and b shows the MOs of **1** which contain the weaker back-bonding interactions involving the $6e_u$, $2a_u$ and $4a_u$ FMOs. Notice that, compared to the interactions illustrated in Fig. 2a and b, less isonitrile $\pi^*$ character is evident in the plots, underscoring the relative weakness of the interaction. Figure 4c and d shows contour plots of the MOs of **1** which contain the metal–

ligand $\sigma^*$ interactions. Notice in the former that the metal–metal component of this MO contains a contribution from the $5e_g$ rhodium FMO and results in the skewed appearance of the Rh—Rh bond. That the $6a_{1g}$ FMO of the rhodium fragment energetically stabilizes this metal–ligand antibonding interaction serves to keep this MO below the Fermi level. As a result of its participation, it is populated with a substantial amount of electron density (0.39 electrons). The other rhodium FMO involved in the forward-donation of density from the isonitrile $\sigma$ orbitals is the antibonding $5d_{z^2}$ interaction, FMO $4a_{2u}$. FMO $4a_{2u}$ is the LUMO of the rhodium fragment, and through the bonding interaction with isonitrile FMO $1a_u$ it receives 0.48 electrons. MO 90 (not shown in Fig. 1) of **1** contains this interaction, and the contour plot is shown in Fig. 4d.

One would expect that the substitution of the electron-withdrawing $CF_3$ group at the para position in the phenylisonitriles with the electron-donating $NMe_2$ group would result in less $\pi$ back-bonding between the rhodium acetate and the axial ligands. Indeed, the results of the calculations on **2**, shown in Fig. 5, corroborate this expectation. Notice that while the magnitude of electron density populating the $4a_{2u}$ and $6a_{1g}$ FMOs as a result of the $\sigma$ forward-donation is nearly identical to that in **1**, the magnitude of the $\pi$ back-donation is significantly reduced. The reason for this reduction is that the $NMe_2$ group, as a $\pi$-donor ligand, destabilizes the isonitirile $\pi^*$ orbitals ($3a_u$ and $3a_g$) through the $\pi$ system of the phenyl ring. The energy splitting between the $5e_g$ rhodium acetate FMOs and the $3a_g$ FMO of the axial ligands is 6.5 eV in **2**, while it is only 4.6 eV in **1**; the net increase in the splitting is 1.9 eV. In contrast, the net increase in the $5e_g - 5a_g$ splitting is only 0.5 eV, since the $5a_g$ (and $5a_u$) isonitrile $\pi^*$ FMO is orthogonal to the delocalized $\pi$ system of the phenyl group and is therefore somewhat insulated from the destabilizing effects of the $NMe_2$ substituent. That the magnitude of the back-donation to the $5a_u$ and $5a_g$ FMOs is larger than that to the $3a_u/3a_g$ set is a consequence of the non-linear Rh—C—N angle and the concomitant symmetry-allowed participation of the $\sigma$ FMOs (vide supra).

It is important to point out that, unlike **1**, the isonitrile $4a_u$ and $4a_g$ FMOs of **2** (not shown in Fig. 5) contain significant $\pi^*$ character and receive 0.02 electrons from the $5e_g$ FMOs of the rhodium fragment. While this interaction certainly contributes to the overall $\pi$ back-donation in **2**, the contribution is minor and does not alter the conclusion that $\pi$ back-donation in this complex is significantly less than that in **1**.

The results of Fenske-Hall calculations on $Rh_2(O_2CH)_4 \cdot (PH_3)_2$, **3**, are shown in Figure 6 and paint a very different picture from that reported previously [9]. Substantial $\pi$ back-donation from the rhodium $5e_g$ FMOs to the phosphine $1b_g$ and $2a_g$ FMOs (labeled in $C_{2h}$ symmetry) is the principal distinguishing characteristic of these results. While the energy splitting between these interacting fragments is 5.6 eV, significant overlap between the phosphorus *dp* hybrid orbitals and the rhodium $5e_g$ FMOs fuels the interaction. The contour plots of MOs 48 and 49, shown in Fig. 7a and b, illustrate the overlap.

To evaluate the reliability of the Fenske-Hall results, a self-consistent-field calculation was performed at the DFT/B3LYP level of theory and the results were examined independent of the orbital model. The deformation density plot shown in Fig. 8 displays the differ-

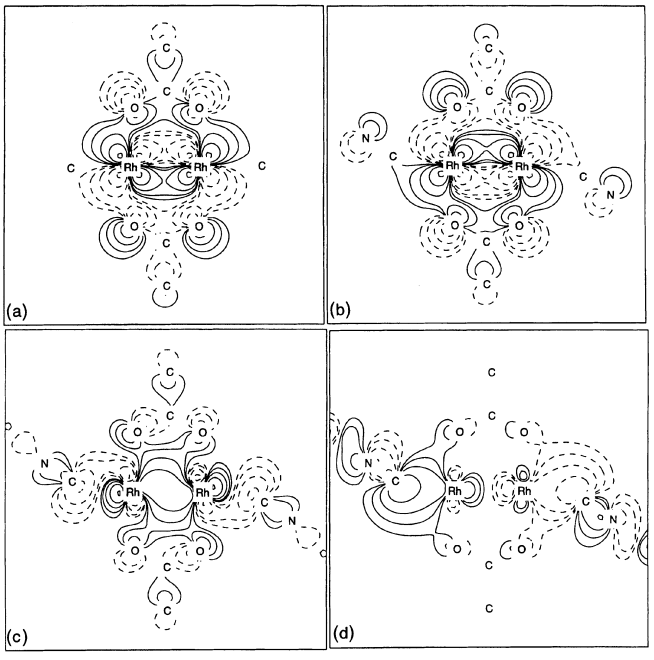


**Fig. 4a–d.** Contour plots for selected MOs of **1**. Planes *A* and *B* correspond to the schematic in Fig. 2. **a** MO 111 in plane *A*. **b** MO 112 in plane *B*. **c** MO 114 in plane *B*. **d** MO 90 in plane *B*. See Fig. 2 for contouring information

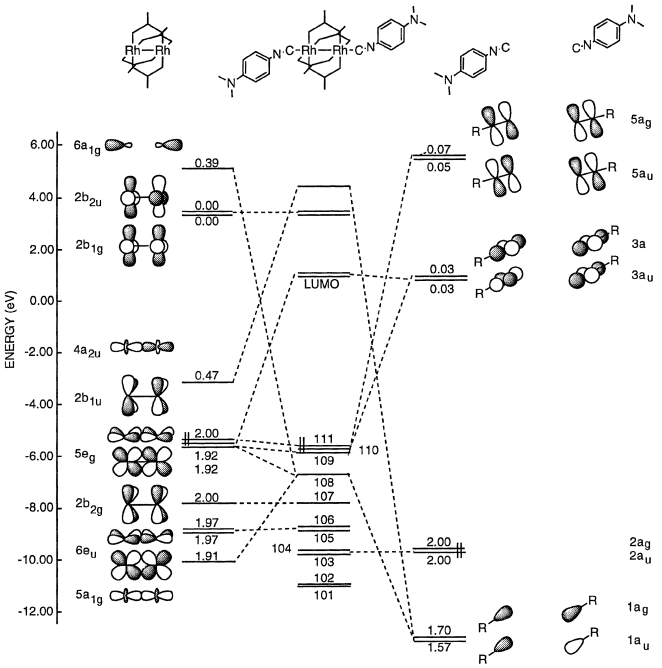


**Fig. 5.** MO diagram for **2** showing the interaction between the $Rh_2(O_2CCH_3)_4$ and $(CNC_6H_4N(CH_3)_2)_2$ fragments

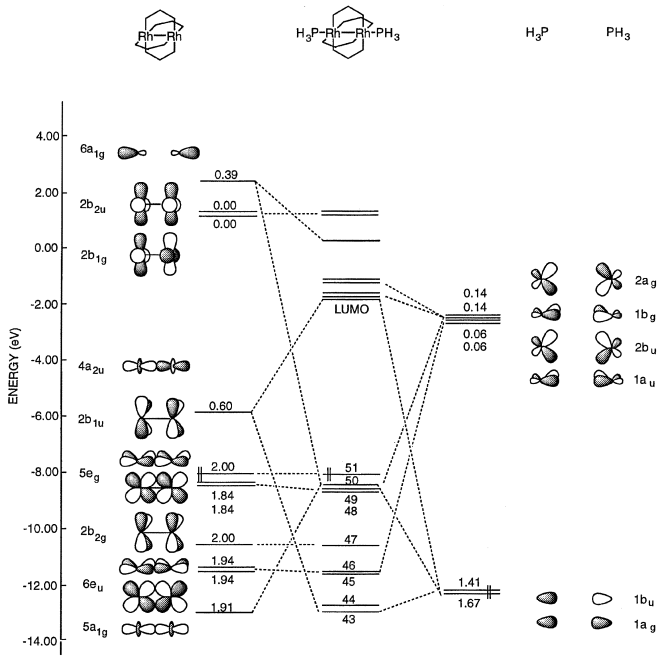


**Fig. 6.** MO diagram for **3** showing the interaction between the $Rh_2(O_2CH)_4$ and $(PH_3)_2$ fragments

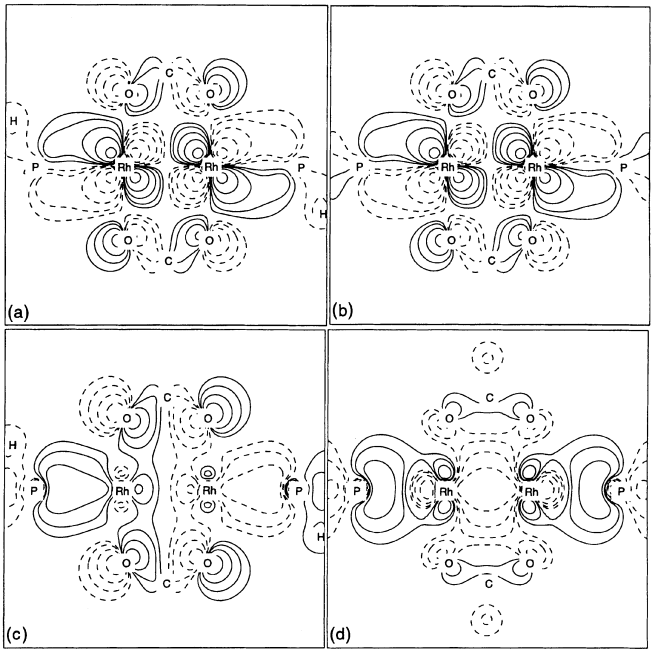


**Fig. 7a–d.** Contour plots for selected MOs of **3**. **a** MO 48, **b** MO 49, **c** MO 43, **d** MO 50

ence between the total molecular density of **3** and the $PH_3$ and $Rh_2(O_2CH)_4$ fragment (or promolecule) densities. Consistent with the Fenske-Hall results, the plot illustrates that the interaction between the metal fragment and the axial ligands results in a depletion of density from the Rh $d\pi$ orbitals and in an accumulation near phosphorus in the Rh—P bonding regions. Note that, by definition, these regions of accumulation cannot

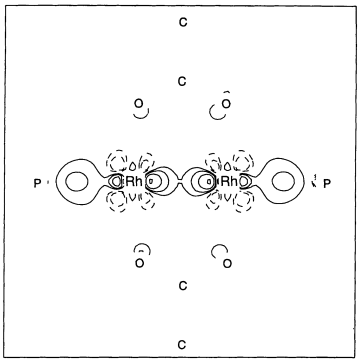


**Fig. 8.** Deformation density plot from an all-electron DFT/B3LYP calculation of **3** where the promolecule densities for the $Rh_2(O_2CH)_4$ and two $PH_3$ fragments were subtracted from the total density of **3**. Nine geometric contours are plotted, the smallest of which is $\pm 0.0003906$ e/*a.u.*[3]

be due to the phosphine lone pair densities since they are part of the promolecule and are subtracted out of the total molecular density [17].

Of secondary interest are the $\sigma$ interactions, the principal components of which are contained within MOs 43 and 50. The latter MO contains the metal-ligand $\sigma^*$ interaction which is stabilized by the rhodium $6a_{1g}$ FMO. Recall that a similar feature was observed in both **1** and **2**. The former MO consists of the HOMO/LUMO interaction in which $\sigma$ density is donated from the phosphine lone pairs to the unoccupied rhodium $4a_{2u}$ FMO. Unlike **1** and **2**, this MO is high enough in energy (due to the relative instability of the $1a_g$ and $1a_u$ FMOs) to be included in Fig. 6. Contour plots of these MOs are shown in Fig. 7c and d.

## 4 Conclusions

To obtain information regarding the structural and electronic makeup of the carbenoid intermediate in catalytic rhodium carboxylate and carboxamide transformations, we have reported electronic structure calculations on a new, structurally stable analog of the intermediate. This analog involves rhodium acetate with phenylisonitrile axial ligation. The isonitrile groups possess $\sigma$ bonding and $\pi$ back-bonding capabilities similar to those of a carbene, yet can be derivatized in the para position of the phenyl group to modulate the electronic character of the ligand. In this study we have capitalized on this ability to modulate the $\pi$ accepting capacity of the isonitrile group to examine the question of $\pi$ back-bonding within the adduct.

Results from Fenske-Hall calculations on **1** and **2** indicate that a significant degree of $\pi$ back-donation occurs between the rhodium fragment and the axial ligands. Previous calculations on related complexes [8, 9] came to the opposite conclusion. Application of the Fenske-Hall method to one of these related complexes, **3**, suggested that $\pi$ back-bonding was, indeed, significant, and raises questions regarding the reliability of these different computational methodologies. Results from a high-level (DFT/B3LYP) calculation corroborate

those from the Fenske-Hall analysis, thereby providing the requisite measure of reliability for the approximate MO method.

During the course of this investigation into the electronic composition of the rhodium acetate isonitriles, a secondary question arose why do the axial ligands bend in **1** and **2**? The computational studies presented herein have not been tailored to provide an answer to this question. Additional calculations which examine the effects of linearizing the axial groups will serve this purpose. Whether the deviation from linearity is a consequence of crystal packing forces or an electronic effect that stems from the participation of metal–ligand $\pi-\sigma$ interactions along with the corresponding $\pi-\pi$ interactions will be analyzed and discussed in a subsequent report.

*Acknowledgements.* A. L. S. thanks the donors of the Petroleum Research Fund, administered by the American Chemical Society (grant 29526-GB6), for partial support of this research and the North Carolina Supercomputing Center for a generous allocation of Cray time.

## References

1. For reviews, see: (a) Doyle MP (1996) Aldrichim Acta 29:3; (b) Padwa A, Austin DJ, Price AT, Semones MA, Doyle MP, Protopopova MN, Winchester WR, Tran A (1993) J Am Chem Soc 115:8669; (c) Adams J, Spero DM (1991) Tetrahedron 47:1765; (d) Maas G (1987) Top Curr Chem 137:75; (e) Doyle MP (1986) Chem Rev 86:919; (f) Doyle MP (1986) Acc Chem Res 19:348
2. (a) Davies HML, Bruzinski PR, Lake DH, Kong N, Fall MJ (1996) J Am Chem Soc 118:6897; (b) Ramos Tombo GM, Bellus D (1991) Angew Chem Int Ed Engl 30:1193
3. (a) Salzmann TN, Ratcliffe RW, Bouffard FA (1980) J Am Chem Soc 102:6161; (b) Melillo DG, Shinkai I, Liu T, Ryan K, Sletzinger M (1980) Tetrahedron Lett 21:2783
4. See Doyle MP, Westrum LJ, Wolthuis WNE, See MM, Boone WP, Bagheri V, Pearson MM (1993) J Am Chem Soc 115:958 and references therein
5. Pirrung MC, Zhang J, Lackey K, Sternbach DD, Brown F (1995) J Org Chem 60:2112 and references therein
6. (a) Dubicki L, Martin RL (1970) Inorg Chem 9:673; (b) Cotton FA, DeBoer BG, LaPrade MD, Pipal JR, Ucko DA (1971) Acta Crystallogr B 27:1664; (c) Norman JG, Kolari H (1978) J Am Chem Soc 100:791
7. Pirrung MC, Morehead AT (1994) J Am Chem Soc 116:8991 and references therein
8. Doyle MP, Winchester WR, Hoorn JAA, Lynch V, Simonsen SH, Ghosh R (1993) J Am Chem Soc 115:9968
9. Bursten BE, Cotton FA (1981) Inorg Chem 20:3042
10. Hall MB, Fenske RF (1972) Inorg Chem 11:768
11. Herman F, Skillman S (1963) Atomic structure calculations. Prentice-Hall, Englewood Cliffs, NJ
12. (a) Bursten BE, Fenske RF (1977) J Chem Phys 57:3138; (b) Bursten BE, Jensen RJ, Fenske RF (1978) J Chem Phys 68:3320
13. Mulliken RS (1955) J Chem Phys 23:1833, 1841
14. Sargent AL, Hall MB (1991) J Comp Chem 12:923
15. Frisch MJ, Trucks GW, Schlegel HB, Gill PMW, Johnson BG, Robb MA, Cheeseman JR, Keith TA, Petersson GA, Montgomery JA, Raghavachari K, Al-Laham MA, Zakrzewski VG, Ortiz JV, Foresman JB, Cioslowski J, Stefanov BB, Nanayakkara A, Challacome M, Peng CY, Ayala PY, Chen W, Wong MW, Andres JL, Replogle ES, Gomperts R, Martin RL, Fox DJ, Binkley JS, Defrees DJ, Baker J, Stewart JJP, Head-Gordon M, Gonzalez C, Pople JA (1995) GAUSSIAN 94, revision D1. Gaussian, Inc., Pittsburgh, Pa
16. Interactive MOPLOT incorporates the programs MOPLOT (Lichtenberger D), PLOTDEN (Bader RFW, Kenworthy DJ, Beddal PM, Runtz GR, Anderson SG), SCHUSS (Bader RFW, Runtz GR, Anderson SG, Biegler-Koenig FW), and EXTREM (Bader RFW, Biegler-Koenig FW) Sherwood P, MacDougall PJ (1989)
17. (a) Coppens P, Stevens ED (1977) Adv Quant Chem 10:1; (b) Low AA, Hall MB (1990) J Phys Chem 94:628 and references therein